ChemSusChem

Research Article
doi.org/10.1002/cssc.202401659

Chemistry Europe
European Chemical Societies Publishing

www.chemsuschem.org

Porous Organic Polymers as Ionomers for High-Performance Alkaline Membrane Water Electrolysis

Sandra Rico-Martínez[+],[a, b] Hyeon Keun Cho[+],[b] Chuan Hu[+],[b, c] Young Jun Lee,[b] Jesús A. Miguel,[a] Angel E. Lozano,*[a, d, e] and Young Moo Lee*[b]

Sustainable hydrogen production is focused on anion exchange membrane (AEM) water electrolyzers (AEMWEs), which still require more development to achieve high performance and durability. Here, we propose a novel class of porous organic polymers (POPs) as durable solid-ionomers for AEMWEs, which was prepared by reacting the 4-methylpiperidone with trifunctional or a mixture of trifunctional:difunctional aromatic monomers (in a 2 : 3 mol ratio). The resulting POP ionomers exhibited exceptional electrochemical properties and remarkable alkaline stability. Particularly noteworthy are the corresponding AEMWEs, which showed an outstanding current density of 13.4 A cm^{-2} at 2.0 V under 80 °C in 1 M KOH solution, which is the highest performance reported in the particulate-ionomers AEMWE state of the art. Moreover, they demonstrated durability at a current density of 0.5 A cm^{-2} for over 500 h with a voltage decay rate of 120 μV h^{-1}. This work offers valuable perspectives on the designing of robust and high-performance solid-state ionomers through low-cost electrophilic aromatic substitution reactions for high-performance energy conversion devices.

Introduction

The pressing nature of the climate emergency, coupled with the depletion of fossil fuel reserves, underscores the critical need for renewable energy alternatives,[1–2] in which green hydrogen is recognized as a viable, environmentally sustainable energy option that has gained substantial interest in recent years.[3] Unlike methods dependent on petroleum processing, green hydrogen production revolves around water splitting through electrolysis, powered by electricity generated from solar power or other renewable sources,[1,4] and it has been suggested as a pathway to achieve carbon neutrality within the coming decades.[5] Traditional alkaline water electrolyzers typically employ highly concentrated alkaline solutions, presenting drawbacks such as accelerated corrosion,[6–7] and vulnerability to ambient CO_2, leading to electrode blockages and reduced conductivity.[8–9] In response to these challenges, polymer electrolyte water electrolysis systems like proton exchange membrane water electrolyzers and AEMWEs have emerged as prominent solutions.[1,10]

The main component of the AEMWE system is the membrane electrode assembly (MEA), consisting of an AEM, ionomers, and catalysts. The AEM acts as a barrier, separating the anode and cathode electrodes to prevent gas crossover,[7] whereas the ionomers act as binders, linking or stabilizing catalyst particles while facilitating ion transport.[11] Over the past decades, significant advancements have been achieved in high-performance AEM development.[12–14] However, the significance of ionomer design often goes unnoticed. Typically, ionomers are chosen with identical or similar structures as AEMs, yet the different working conditions of AEMs and ionomers require different properties.[15] Ionomers must possess high water and gas permeability, electrochemical stability, and low catalyst adsorption ability.[6,16]

AEMWE systems are primarily based on hydrocarbon-based polymer electrolytes due to the challenges in stabilizing the junction point of the electron-withdrawing perfluoroalkyl chain and quaternized functional groups.[17] Conversely, hydrocarbon ionomers easily adhere to catalyst surfaces and are susceptible to oxidation at high electrochemical potentials, which can compromise the performance and durability of electrochemical devices. To mitigate the detrimental effects of ionomer oxidation, various strategies have been explored to design high-performance AEMWEs including: utilizing ionomer-free electrodes, designing particulate ionomeric binders, employing ionomeric binders with low adsorption energy, or applying competitive adsorption techniques.[18] The use of particulate ionomers in place of conventional solution-processed thin-film ionomer electrodes is considered as an innovative approach to

[a] IU CINQUIMA, Department of Inorganic Chemistry, Faculty of Science, University of Valladolid, Valladolid, Spain
[b] Department of Energy Engineering, Hanyang University, Seoul, South Korea
[c] School of Energy and Environment, Southeast University, Nanjing, China
[d] Institute of Polymer Science and Technology, ICTP-CSIC, Madrid, Spain
[e] Surfaces and porous materials (SMAP), University of Valladolid, Valladolid, Spain

Correspondence: Angel E. Lozano, IU CINQUIMA, Department of Inorganic Chemistry, Faculty of Science, University of Valladolid, 47011 Valladolid, Spain.
Email: lozano@ictp.csic.es

Young Moo Lee, Department of Energy Engineering, Hanyang University, Seoul 04763, South Korea.
Email: ymlee@hanyang.ac.kr

[+] These authors contribute equally to this work.

Supporting Information for this article is available on the WWW under https://doi.org/10.1002/cssc.202401659

minimize undesirable ionomer-catalyst interactions.[19] Typically, insoluble ionomers such as quaternized ethylene tetrafluoroethylene (ETFE)[20–21] and polynorbornene[22] are employed in particulate ionomeric binders. These ionomers feature phenyl-free polymer backbones, resulting in lower adsorption energy with good oxygen evolution reaction activity of catalysts.[23] Additionally, the particulate state reduces direct contact with catalysts, further mitigating potential adverse interactions.

Alternative methods to achieve high-performance AEMWEs have been widely explored, including crosslinking, grafting, block copolymer structures, and high free volume fraction polymers.[24–25] However, these techniques often face limitations, either in the choice of polymer backbone or the complex synthesis procedures. Chuan et al. developed highly rigid triptycene-branched polyelectrolytes utilizing a poly(fluorene/dibenzyl-co-aryl piperidinium) backbone. The resulting triptycene-based AEMWE achieved superb current density record of 16 A cm^{-2} at 2.0 V and 80 °C along with a stable operation at 60 °C under 1.5 A cm^{-2} for 2000 h. The excellent results suggest that the triptycene-branched polymers are promising candidates for future AEMWE applications.[6]

Porous organic polymer (POP) materials have recently gained significant interest for various applications, including energy storage,[26] gas sorption,[26–27] gas separation,[28] and catalysis[29] among others. This attention stems from their notable properties such as high specific surface area, customizable pore size, and facile functionalization. Synthesizing POPs is made feasible through a cost-effective methodology involving electrophilic aromatic substitution (EAS) reaction between ketones with electron-withdrawing groups and trifunctional rigid aromatic monomers by employing a superacid as the promoter. The resulting POPs exhibit remarkable microporosity, Brunauer–Emmett–Teller (BET) surface areas reaching up to 800 m^2 g^{-1}, along with exceptional thermal stability surpassing 450 °C, coupled with high gas uptake capabilities.[26] Inspired by the excellent properties of POPs, we designed a series of POP-based alkaline ionomers for AEMWEs using 4-methylpiperidone (MeP) and different trifunctional (or mixtures trifunctional: bifunctional) aromatic monomers employing trifluoromethanesulfonic acid (TFSA) as acid catalyst as summarized in Figure 1. Changes in the arene and ketone monomers may bring changes in the resulting properties, which will lead us to optimize the best POP structure for the fabrication of high-performance and long-term durability AEMWEs. Thus, the objective of this research is to examine the effects of POP structures and properties such as ionic exchange capacity (IEC), water uptake, alkaline stability, and water electrolysis performance of the resulting ionomers.

Experimental Section

Materials

Triptycene (TRP, 98 %), p-terphenyl (TP, > 99.5 %), iodomethane (MeI, 99 %), anhydrous dichloromethane (DCM, > 99.8 %), N-methyl-2-pyrrolidone (NMP, 99.5 %), and potassium carbonate (K_2CO_3, 99 %) were obtained from Sigma Aldrich (Darmstadt, Germany). 1,3,5-triphenylbenzene (TPB, > 99 %), trifluoroacetophenone (TFAP, > 98 %), biphenyl (BP, > 99.5 %), and 4-methylpiperidone (MeP, > 98 %) were acquired from TCI Development Co. Ltd (Tokyo, Japan). Trifluoroacetic acid (TFA, 99.0 %) was purchased from Daejung (Busan, South Korea). Trifluoromethanesulfonic acid (TFSA, > 99 %) was obtained from UIV CHEM

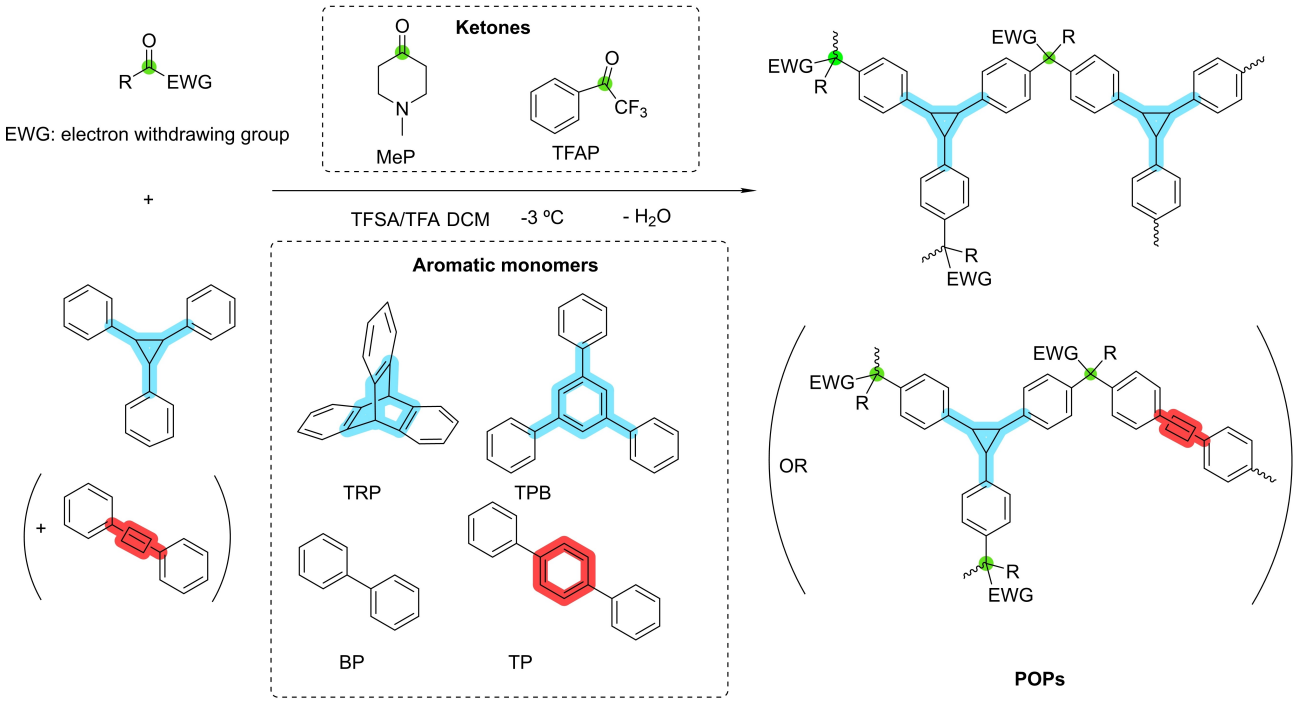

Figure 1. Schematic representation of the synthesis of POPs.

(Shanghai, China). All reagents were used as received with no further purification.

Methods

Thermal Properties

The thermal stability of POPs was carried out by thermogravimetric analysis (TGA) using a TA–Q500 instrument (TA, New Castle, DE, USA), operated under an N_2 atmosphere (60 mL min^{-1}) from 30 to 850 °C with sensitivity and resolution parameters set to 1 and 4, respectively.

Structural Analysis

The chemical structures of synthesized POPs and POP-MeCl polymers were determined using Fourier-transform infrared (FT-IR) spectroscopy and solid-state ^{13}C cross-polarization magic angle spinning NMR (CP-MAS ^{13}C NMR). FT-IR spectroscopy of POPs and POP-MeCl was carried out in an apparatus (Danbury, CT, USA) with an attenuated total reflection accessory (ATR-FTIR) and on a PerkinElmer Spectrum RX–I FTIR spectrometer (Waltham, MA, USA), respectively. CP-MAS ^{13}C NMR of POPs and POP-MeCl were recorded on a Bruker BioSpin GmbH spectrometer operating at a Larmor frequency of 126 MHz and 100 MHz, spinning the sample at 5 kHz and at 11 KHz, respectively.

Porosity Measurements

The porous texture analysis of the POPs involved examining their N_2 adsorption-desorption isotherms at −196 °C (77 K) using a volumetric ASiQwin device (Quantachrome) across a relative pressure (P/P0) range of 10^{-6} to 1.0. Prior to sorption measurements, samples underwent a 12-h degassing at 180 °C under vacuum to eliminate any residual sample humidity and adsorbed gases. The adsorption curve of the isotherms was utilized to determine the apparent surface area (S_{BET}) employing the Brunauer-Emmett-Teller (BET) method within the 0.01 to 0.2 P/P_0 range. The pore average was estimated in N_2 adsorption at −196 °C by the BJH method. The CO_2 adsorption capacities of the POP-MeCl at 25 °C (298 K) were measured in a volumetric device 3Flex Version 5.02 (Micromeritics). Samples were degassed at 100 °C for 12 h under vacuum before the CO_2 adsorption measurements.

Morphological Analysis

Morphological texture of the POP-MeCl was examined using field emission scanning electron microscopy (FE-SEM) using a HITACHI–S4800 microscope on Pt-metallized sample operating at an acceleration voltage of 1.5 kV under high vacuum. For the preparation of the samples, about 10 mg of POP-MeCl powders were dispersed in an ultrasonic bath at < 5 °C for 90 min in 2 mL EtOH. Later, 0.5 mL from the middle of the dispersion were taken and diluted to 2 mL EtOH.

Transmission electron microscopy (TEM) images of the POP-MeCl and catalyst (IrO_2 or PtRu/C) were acquired in a TEM-2 JEM 2100 F JEOL equipped with EDS apparatus operated at 200 kV. For the preparation of the samples, POP-MeCl (in a 20 wt% or 30 wt%) and catalyst powders were dispersed in an ultrasonic bath at < 5 °C for 90 min in 2 mL IPA. Later, 0.5 mL from the middle of the dispersion were taken and diluted to 2 mL IPA.

Water Uptake and IEC

Water uptake (WU) of POP-MeCl was determined by gravimetric analysis at 25, 60, and 80 °C. First, the samples were immersed in deionized water with stirring at specified temperature for 24 h. The hydrated mass (M_{hyd}) was recorded after wiping the excess water from the surface of the sample by filtering. After that, the sample was dried at 120 °C for 24 h to completely remove the absorbed water, and the dry mass was recorded as M_{dry}. The WU of the samples in Cl^- form could be calculated as follows.

$$WU\ (\%,\ Cl^-) = \frac{M_{hyd} - M_{dry}}{M_{dry}} \times 100$$

The IEC of the samples was determined using a titration method. The dried POP-MeCl samples were immersed in 20 mL 0.1 M $NaNO_3$ at 25 °C for 24 h to release Cl^- ions. Subsequently, a 5 wt% K_2CrO_4 aqueous solution was added acting as the indicator. Finally, the mixture solution was titrated with 0.01 M $AgNO_3$ solution after the observation of the first orange drop. The IEC (Cl^-) of the samples can be calculated using the following equation.

$$IEC\ (mmol\ g^{-1},\ Cl^-) = \frac{C_{AgNO3} \times V_{AgNO3}}{M}$$

where $V_{AgNO3}$is the $AgNO_3$ consumed during the titration process; and *M*is the dry weight of the sample before titration.

Membrane Electrode Assembly Preparation

The MEA was prepared by employing IrO_2 (Alfa Aesar, MA, USA) as anode catalyst, PtRu/C (Alfa Aesar, MA, USA, 40 wt% Pt, 20% Ru) as cathode catalyst, poly(dibenzyl-co-terphenyl piperidinium) (PDTP, 25 μm) as the AEM,[12,30] and POP-MeCl as ionomers at both sides of the membrane. Before preparing the catalyst ink, the POPs powders were ground in a mortar, and then mixed with catalyst, deionized water, and isopropanol in a glass vial. Subsequently, the catalyst ink was dispersed in an ultrasonic bath at < 5 °C for 90 min, and then automatically sprayed onto the surface of a PDTP AEM to prepare catalyst-coated membranes (CCMs) using a hand-made automatic spraying machine (see Figure S1). The catalyst loading amounts at the cathode and anode were fixed to 1.0 mg cm^{-2} of PtRu/C

and 2.0 mg cm^{-2} of IrO_2, respectively, and the POP loadings were 10 wt%, 20 wt%, or 30 wt%. The CCMs were then immersed in a 1 M KOH solution at 60 °C for 24 h. Finally, the CCMs were assembled with porous transport layers (PTLs), gaskets, and bipolar plates. Anode and cathode PTLs were composed of nickel fiber plate (Dioxide Materials, USA) and carbon paper (SGL 22 BB), respectively. A gold-coated Ni plate and a graphite plate with an effective area of 5 cm^2 served as bipolar plates at the anode and cathode, respectively.

Water Electrolysis Measurements

Water electrolysis performance was carried out using a dry cathode approach tailored for industrial demands. On the anode side, a 1 M KOH solution was supplied at a flow rate of 36 mL min^{-1}. I–V curves of AEMWE were assessed utilizing a potentiostat (Bio-Logic HCP- 803) coupled with a current booster (VMP3 Booster, Biologic SAS, Grenoble, France, 80 A) across a voltage range from 1.35 to 2.0 V, with a voltage scan rate of 5 mV s^{-1}. Each voltage point was sustained for 10 s. Potentiostatic electrochemical impedance spectroscopy (EIS) was conducted at 1.6 V and 1.8 V at 80 °C and 60 °C over a frequency spectrum of 1 Hz–200 kHz. The in-situ durability of the water electrolysis system was appraised utilizing a charging system (LAND Battery Testing System, CT3002 N, China) under a constant current density of 0.5 A cm^{-2} at 60 °C for 500 h.

Synthesis of POPs

Five different POPs were synthesized by EAS reaction between a ketone and an aromatic monomer employing mixture of TFSA/TFA (in a molar ratio 100:17) as the catalyst and solvent at −3 °C (see Figure 1). DCM was added in a 3:1 molar ratio to the mixture of acids. The typical ketone monomer used in this work was MeP, or a mixture of MeP with TFAP, whereas the aromatic monomer was a trifunctional aromatic ring, or a blend with a difunctional monomer in a 2:3 molar ratio. Table 1 summarizes the monomer ratio employed for the synthesis of POPs Thus, two homopolymers were synthesized between the reaction of MeP ketone and a trifunctional aromatic monomer (TRP or TPB) in a 3:2 molar ratio, which are denoted as POP1 and POP2, respectively. Additionally, to decrease the number of piperidone groups in the polymer, a copolymer (POP3) was made by mixing MeP and TFAP ketones in equimolecular electrophilic amounts and employing TRP as a nucleophile in a 3:3:4 molar ratio, respectively. Finally, with the idea of adjusting the characteristics of the system, copolymers were obtained by reacting MeP with a mixture of equivalent amounts of a bifunctional nucleophilic monomer (BP or TP) and the trifunctional monomer TRP, (named POP4 and POP5, respectively) in a molar ratio of 6:3:2.

All POPs were obtained in quantitative yields. The chemical structure of the POPs synthesized in this work is displayed in Figure 2. Details of the synthesis of POPs are described in the Supporting Information section. As an example, the synthesis of POP4 is described as follows: An oven-dried three-necked Schlenk flask (500 mL), equipped with a mechanical stirrer blanketed by a nitrogen dynamic flow, was charged with TRP (1.6107 g, 6.30 mmol), BP (1.4650 g, 9.50 mmol), MeP (2.3370 mL, 19.0 mmol) and anhydrous DCM (40 mL). The mixture was cooled down to −3 °C followed by adding chilled TFA (2.3 mL), and chilled TFSA (15.2 mL) with a dropping funnel for about 30 min. Subsequently, the mixture was maintained at −3 °C with mechanical stirring for 96 h. After that, the reaction mixture was quenched by adding cool water. The precipitated solid was filtered and then neutralized by washing with $NaHCO_3$ solution, deionized water, ethanol, and dichloromethane several times. Finally, an orange powder with a quantitative yield of 99% was obtained after drying at 180 °C under vacuum for 24 h.

Table 1. Molar ratio of monomers employed in the synthesis of POPs.

POPs	Ketone		Trifunctional monomer		Bifunctional monomer	
	MeP	TFAP	TRP	TPB	BP	TP
POP1	3	–	2	–	–	–
POP2	3	–	–	2	–	–
POP3	3	3	4	–	–	–
POP4	6	–	2	–	3	–
POP5	6	–	2	–	–	3

Quaternization of POPs

POP (3.80 mmol of piperidone groups) powders were mixed with 20 mL NMP in a 70 mL flask with a magnetic stirrer. Subsequently, K_2CO_3 (11.30 mmol, 1.56 g) and MeI (11.30 mmol, 0.71 mL) were added to the flask and reacted at room temperature for 24 h under a dark environment. Later, the suspension was filtered, and a light-orange powder was obtained. The powder was washed with deionized water three times to remove the residual salts and then immersed in a 1 M NaCl solution for 24 h to exchange I^- ions to Cl^-. Finally, the powder

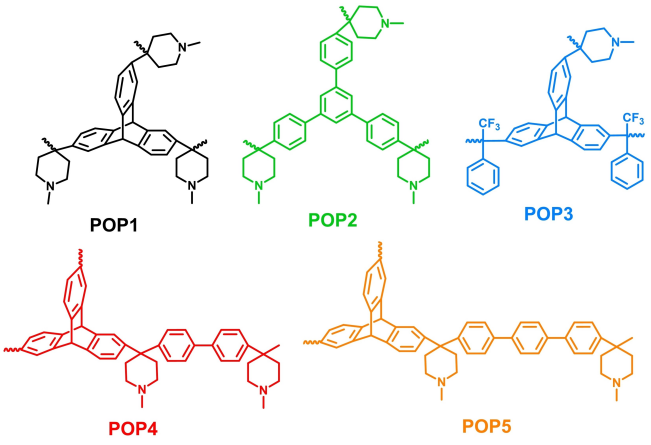

Figure 2. Chemical structure of POPs in this study.

defined as POP-MeCl was dried in a vacuum oven at 120 °C for 24 h. The detailed synthesis process of each POP-MeCl has been specified in the Supporting Information section.

Results and Discussion

Polymer Functionalization and Characterization

The chemical structure of the prepared POPs and POP-MeCl was evaluated by FTIR as shown in Figure 3a and Figure S2. The band at 1677 cm^{-1} corresponded to the benzene ring in the polymer backbone, the peak at 1472 cm^{-1} was associated with the methyl group[31] and the band at 1380 cm^{-1} to the stretching C–N bond.[31] The quaternization of the POPs could be determined by the peak at 980 cm^{-1}, attributed to the methyl groups on the quaternary salt ($C–N^+$).[32] POP3 showed additional peaks at 1234 and 1130 cm^{-1}, which corresponded to C–F stretching bands.[26]

The chemical structure of the synthesized POPs and POP-MeCl was confirmed by CP-MAS ^{13}C NMR as shown in Figure 3b and Figure S3, respectively. The peaks at 100–160 ppm were assigned to the carbon atoms in the aromatic rings, and the peaks at 25–70 ppm were attributed to MeP moiety. The peak at 62 ppm (C9) was ascribed to the quaternary atom at the MeP moiety formed during the reaction. The peaks at 43 ppm and 30 ppm come from the $-CH_2$ (C10-13) and $-CH_3$ (C14) groups of the MeP, respectively. In the case of POPs derived from TRP, an additional peak at 53 ppm was attributed to the quaternary carbons of the TRP moiety (C1, C8). The successful quaternization of the POPs could be confirmed by the increase in the C14 relative intensity compared to C10-13 in POP-MeCl as Figure S4 shows.

Thermal stability of the synthesized POPs was evaluated by TGA under a N_2 atmosphere. As shown in Figure 4, POPs presented high thermal stability, superior to 400 °C with moderate char yields at 800 °C (varying from 32 to 65 %). Decreasing the amount of MeP (in POP3), higher char yields (65 % and 36 % for POP3 and POP1, respectively) and degradation temperature (values of 433 °C and 403 °C were observed for POP3 and POP1, respectively) were obtained as can be seen in Table S1.

When the tertiary amine nitrogen atoms of the POPs were quaternized, a weight loss was observed at 200 °C and above

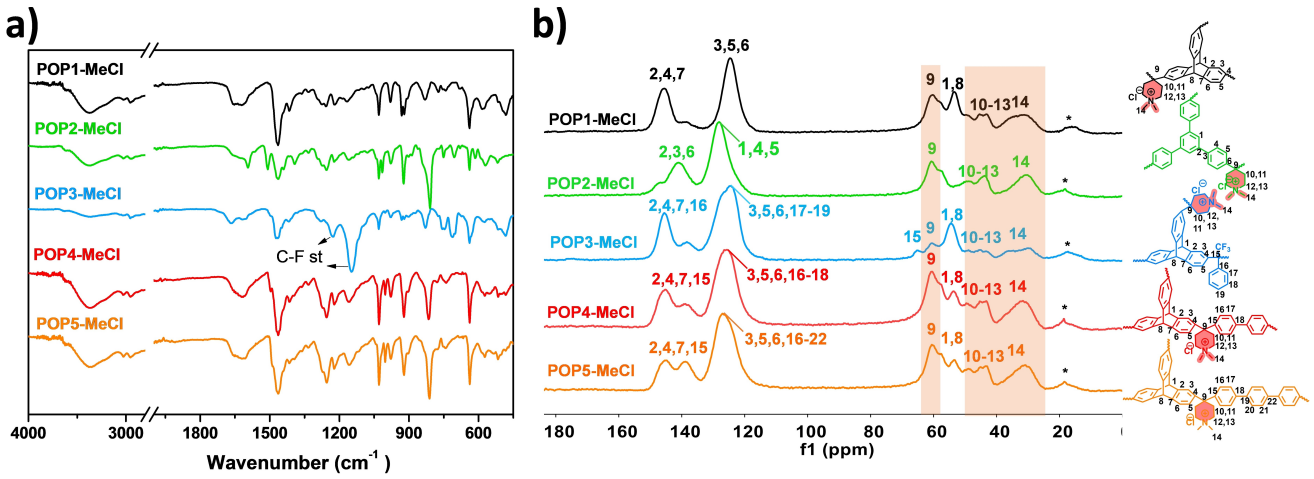

Figure 3. a) ATR-FTIR spectra and b) CP-MAS ^{13}C NMR spectra of POP-MeCl. *Spinning side bands.

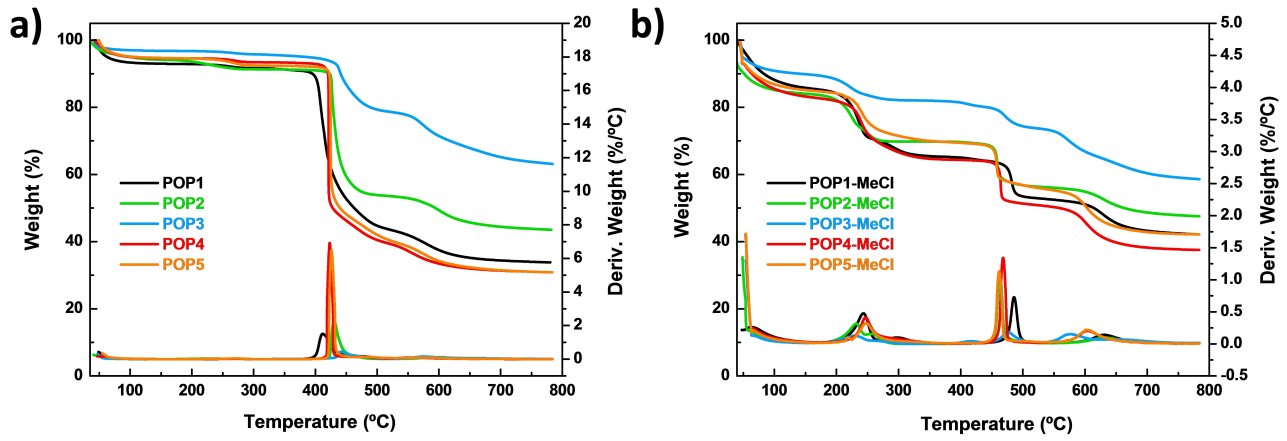

Figure 4. TGA curves of POPs and POP-MeCl before (a) and after (b) quaternization.

due to the loss of MeCl entities, which further confirmed the quaternization of the piperidone nitrogen. Table S2 shows the theoretical and experimental weight loss from 200 to 350 °C and its quaternization functionalization degree, according to the complete quaternization of piperidone groups. In all the cases, the functionalization achieved was higher than 85%.

The porous properties of the obtained POPs were evaluated by N_2 and CO_2 adsorption. The specific surface area values and N_2 isotherm of all POPs seem to demonstrate that the diffusion of N_2 through the pores is hindered (Table S3 and Figure S5). This fact led us to analyze the gas adsorption isotherms employing a smaller-size molecule: CO_2 (Figure 5). It should be noted that even though the N_2 adsorption was very low, the CO_2 adsorption was similar to other analogous POPs derived from TRP or 1,3,5-triphenylbenzene, which presented large BET surface areas.[26] Also, the use of TFAP, as a comonomer, seems to increase gas adsorption[26,33] while the use of bifunctional comonomers (BP or TP), produces a decrease in gas adsorption.

The surface morphology of the synthesized POP-MeCl was evaluated by FE-SEM images (Figure S6). POP-MeCl consisted of clusters of small nanoparticles with sizes lower than 100 nm.

TEM images of the dispersion of the different POP-MeCl ionomers (20 wt%) and IrO_2 catalyst are included in Figure S7, in which particle sizes of each POP are in the range of 1–2 μm within the catalyst particles evenly distributed on the surface of ionomers. Figure S8 shows a comparison of the TEM images of the highest WE performance POP ionomer, POP3-MeCl, with IrO_2 and with PtRu/C catalyst, in a 20 and 30 wt%, in which higher catalyst agglomerations were observed in the case of 30 wt% of POP3-MeCl with IrO_2. Additional TEM-EDS were carried out for POP1-MeCl and POP3-MeCl (Figures S9 and S10), showing a homogeneous distribution of the catalyst in the POP particles with no obvious aggregation.

IEC and Water Uptake

The ionic exchange capacity (IEC) of the polymers was highly dependent on the structure of the POPs. IEC values of the POP-MeCl are presented in Table 2 and varied from 1.8 to 3.4 mmol g^{-1}. Homopolymers derived from TRP presented higher IEC values than the one derived from TPB as observed for POP1-MeCl (3.2 mmol g^{-1}) and POP2-MeCl (2.9 mmol g^{-1}). This tendency has already been described.[6] Copolymers incorporating bifunctional monomers to the trifunctional TRP showed that by adding BP (POP4-MeCl), the IEC value remained constant (3.2 mmol g^{-1}), whereas a decrease in the IEC to 2.9 mmol g^{-1} value compared to the homopolymer POP1-MeCl was observed using TP (POP5-MeCl). In contrast, POP3-MeCl possessed the lowest IEC value (1.8 mmol g^{-1}) due to the lower content of MeP because of the use of TFAP ketone as comonomer.

The WU of the POP-MeCl increased with IEC as typically happens (Figure 6).[21] Thus, the POP-MeCl with the highest IEC value (3.2 mmol g^{-1}), POP1-MeCl and POP4-MeCl, showed the highest WU (540% at 25 °C), followed by POP5-MeCl (364% at 25 °C) and POP2-MeCl (247% at 25 °C), with an IEC of 2.9 mmol g^{-1}. Analogously, POP3-MeCl, which presented the lowest IEC value (1.6 mmol g^{-1}) showed the lowest WU (150% at 25 °C). As the water is the reactant at the cathode and the carrier of ion transport, a higher WU is supposed to enhance the electrode reaction and OH^- transport.

Table 2. The ion exchange capacity of POP-MeCl.

POP-MeCl	IEC exp. (theoretical) mmol g^{-1}
POP1-MeCl	3.3±0.3 (3.2)
POP2-MeCl	3.0±0.2 (2.9)
POP3-MeCl	1.8±0.1 (1.6)
POP4-MeCl	3.4±0.1 (3.2)
POP5-MeCl	3.0±0.1 (2.9)

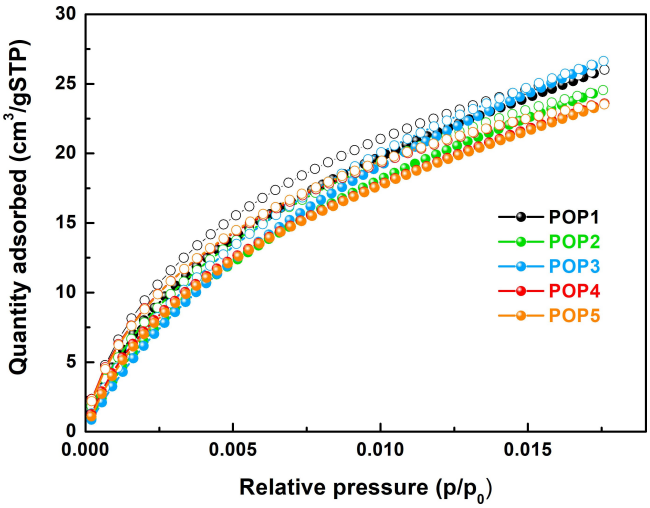

Figure 5. CO_2 adsorption (full symbols)−desorption (empty symbols) of POPs at 25 °C.

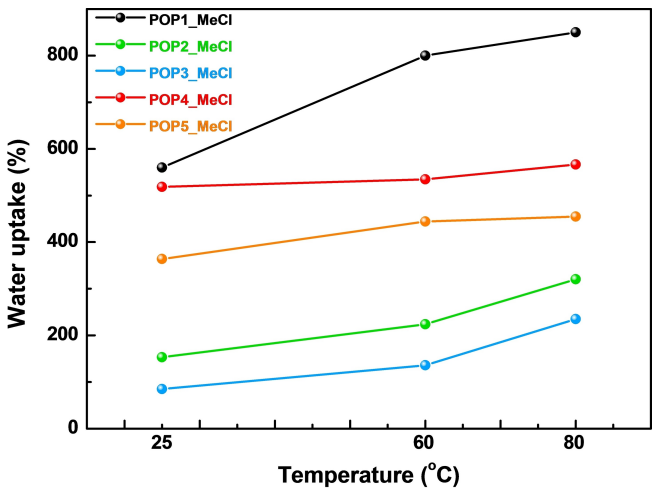

Figure 6. Water uptakes at 25 °C, 60 °C and 80 °C of POP-MeCl.

AEMWE Performance

Impact of Ionomer Species

The water electrolysis performance was evaluated employing the different synthesized POP-MeCl as ionomers in a 1 M KOH solution using IrO_2 and PtRu/C as the anode and cathode catalysts, respectively, and a PDTP AEM with a thickness of 25 μm, which possesses excellent WE performance.[12] The impact of the ionomer POP was evaluated based on loads of 20 wt% POP-MeCl compared to the catalysts. As shown in Figures 7a and b, POP3-MeCl presented the highest current density of 13.4 A cm^{-2} at 2.0 V and 80 °C, along with a low Ohmnic resistance (R_{Ohm}) of 0.02203 Ω cm^{-2} and a charge

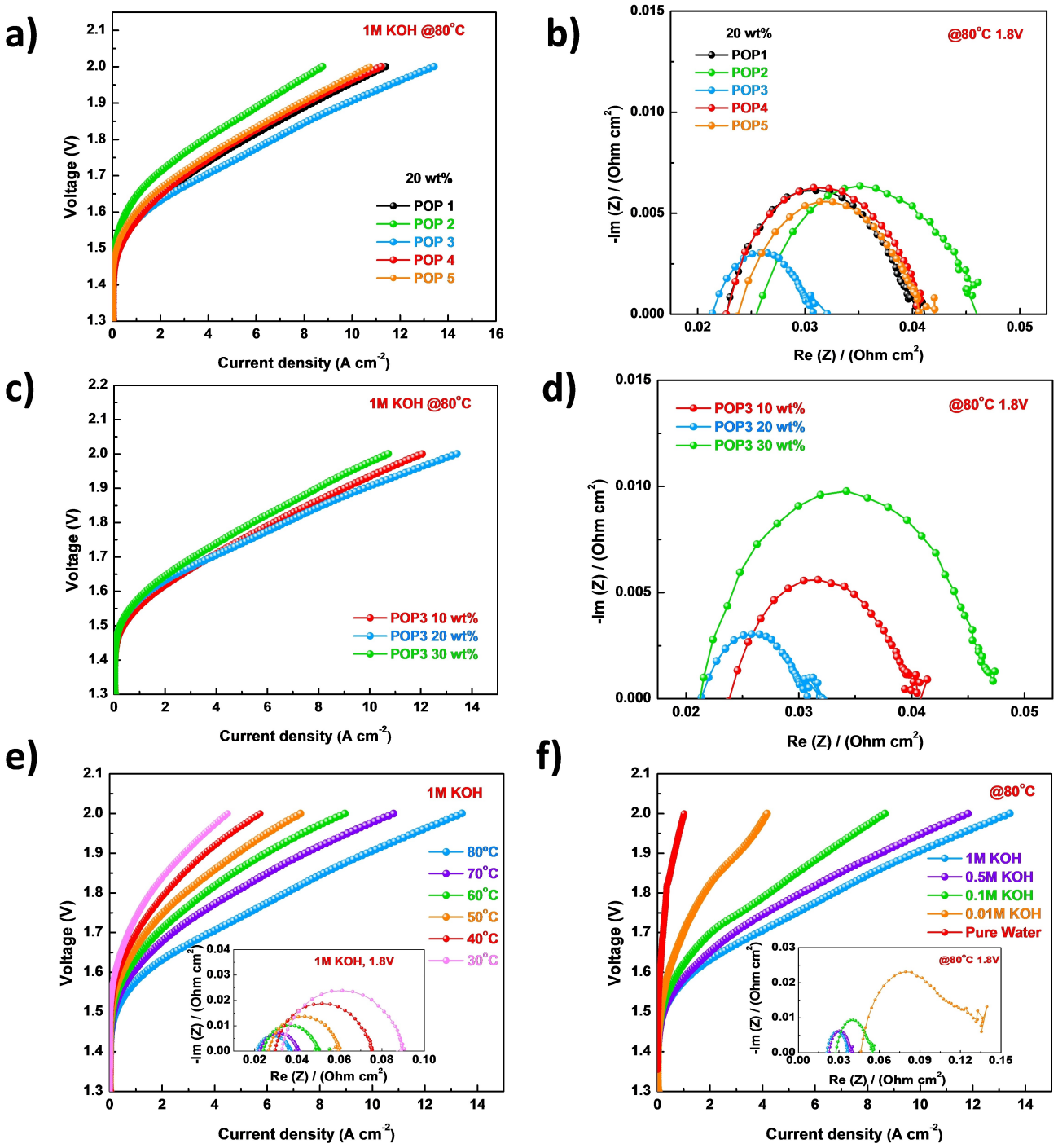

Figure 7. Impact of the ionomer species on AEMWE performance. a) I–V curves, b) EIS spectra at 80 °C and 1.8 V of AEMWE with different POP-MeCl (20 wt%) as ionomers. Impacts of the ionomer contents on AEMWE performance c) I–V curves, d) EIS spectra at 80 °C 1.8 V of AEMWE with different POP3-MeCl ionomer contents. e) Impact of the temperature on POP3-MeCl-based AEMWE performance (20 wt%) e) I–V curves and EIS at 1.8 V, f) impact of the KOH concentration on POP3-MeCl-based AEMWE performance (20 wt%): I–V curves and EIS at 80 °C and 1.8 V. Test conditions: PDTP AEM (25 μm), 2 mg cm^{-2} IrO_2 at the anode, 0.7 mg cm^{-2} PtRu/C at the cathode, 80 °C, 1 M KOH.

transfer resistance (R_{CT}) of 0.01087 Ω at 1.8 V (Figure 7b), compared with AEMWEs using POP1-MeCl (9.7 A cm^{-2}, R_{Ohm} of 0.02274 Ω cm^{-2} and R_{CT} 0.01799 Ω cm^{-2}), POP5 (11.2 A cm^{-2}, R_{Ohm} of 0.02384 Ω cm^{-2} and R_{CT} 0.01835 Ω cm^{-2}), POP4-MeCl (10.7 A cm^{-2}, R_{Ohm} 0.02274 Ω cm^{-2} and R_{CT} 0.01826 Ω cm^{-2}), and POP2-MeCl (8.8 A cm^{-2}, R_{Ohm} 0.02548 Ω cm^{-2} and R_{CT} 0.02073 Ω cm^{-2}). Better WE performance was achieved with POP-based AEMWEs with TRP in the structure (POP1) compared to TPB (POP2), as was previously reported.[6] Analogous results were obtained operating at 60 °C (Figure S12). Unexpectedly, the POP with lower IEC and WU values presented superior performance in ionomer-based AEMWE, which could be associated with the low charge transfer resistance of 0.01087 Ω cm^{-2} and 0.03126 Ω cm^{-2} at 1.8 V and 1.6 V, respectively. Charge transfer resistance and the catalyst layer activity depend on the cation adsorption and the phenyl adsorption. The cation adsorption on catalyst surface is much stronger than phenyl adsorption.[34] As POP3-MeCl has hydrophobic $-CF_3$ group, and shows the increase in the ionomer adsorption energy on catalyst surface, POP3-MeCl incorporated catalyst layer has higher catalytic activity and show better water electrolysis performance. This finding had already been reported for fluorene ionomers and ETFE-grafted ionomers that the enhanced performance of the lowest IEC materials was attributed to the lower adsorption of phenyl and ammonium groups onto the catalyst surface.[18,21] The presence of biphenyl and terphenyl groups in POP4 and POP5 increases the adsorption onto the catalyst surface. To the best of our knowledge, the current density achieved at this work (13.4 A cm^{-2} at 2.0 V and 80 °C) employing the particulate ionomer POP3-MeCl is the highest recorded in solid ionomers based-AEMWEs.[18,21,35–36]

Effect of Ionomer Content

The impact of the ionomer content was evaluated employing the highest WE performance ionomer, POP3-MeCl, based on loads of 10, 20 and 30 wt% compared to the catalysts, using a PDTP membrane with a thickness of 25 μm (Figure 7c). The increase in the ionomer amount from 10 to 20 wt%, resulted in an improvement in the current density at 2 V and 80 °C (from 10.7 A cm^{-2} to 13.4 A cm^{-2}, respectively). EIS (Figure 7d) also indicates that the R_{Ohm} decreased from 0.02388 to 0.02203 Ω cm^{-2} along with a substantial decrease in R_{CT} (from 0.01697 to 0.01087 Ω cm^{-2}) after increasing the ionomer content from 10 wt% to 20 wt%. However, increasing the POP3-MeCl amount to 30 wt% did not result in an improvement in WE performance (the current density achieved was 12.1 A cm^{-2}), showing considerable higher R_{CT} (0.02609 Ω cm^{-2}), presumably due to the higher catalyst particle agglomeration in the POP particles as shown in Figure S8. Moreover, excessive ionomer concentration could increase gas transport resistance and diminish active sites on the catalyst layer, thereby decreasing WE performance.

Effect of Temperature and KOH Concentration

The impact of the temperature in the range from 30 to 80 °C and the influence of the alkaline concentration were analyzed employing the highest WE performance ionomer, POP3-MeCl, based on loads of 20, compared to the catalysts, using a PDTP membrane with a thickness of 25 μm. The current density decreased with the temperature due to the increase in R_{Ohm} and R_{CT} (Figure 7e). Figure 7f shows the dependence of WE performance on KOH concentration in pure water, 0.01 M, 0.1 M and 1 M KOH. When operating in a concentrated alkaline solution, the AEMWE exhibited a higher current density attributed to the improvement in conductivity (the current densities achieved were 1.0, 4.2 and 13.4 A cm^{-2} in pure water, 0.01 M KOH and 1 M KOH, respectively).

In-situ *Durability Measurement*

The *in-situ* durability of the highest WE performance POP1-MeCl and POP3-MeCl-based AEMWEs was evaluated at a constant current density of 0.5 A cm^{-2} for 500 h at 60 °C in 1 M KOH. As shown in Figure 8, the POP1-based AEMWE showed an initial voltage of 1.69 V, which then gradually increased to 1.75 V during the following 500 h (see Figure 8a). The total voltage decay rate was 120 μV h^{-1}, well below that of most state-of-the-art AEMWEs. POP3-based AEMWE experienced similar deterioration (Figure 8b) with a voltage decrease from 1.61 V to 1.68 V compared to POP1-based AEMWE under the same operation conditions, with a voltage decay rate of 140 μV h^{-1}. The voltage of POP3 was lower than 1.7 V during the test. A high operation voltage is not economical for industrial use since this indicates that the AEMWE system requires high energy to carry out water splitting.

Conclusions

In this work we proposed the use of POPs as durable solid ionomers. These POPs were made by reacting 4-methylpiperidone with a trifunctional monomer or with a mixture of trifunctional:difunctional aromatic monomers (2:3 mol ratio). The synthesized POPs showed high thermal and chemical stability along with excellent electrochemical properties. POP3-containing AEMWEs, which showed the lowest IEC values achieved a remarkable current density of 13.4 A cm^{-2} at 2.0 V under 80 °C in a 1 M KOH solution and could continuously operate at a current density of 0.5 A cm^{-2} for more than 500 h with a low voltage decay rate of 120 mV h^{-1}. This is the highest performance recorded in the particulate-ionomers AEMWE state of the art. Conversely, POP1-based ionomer having higher IEC value displayed an inferior current density of 9.7 A cm^{-2} with a high voltage decay rate of 140 μV h^{-1}. This research provides insights into the design of durable solid-state ionomers using low-cost EAS for high-performance AEMWEs.

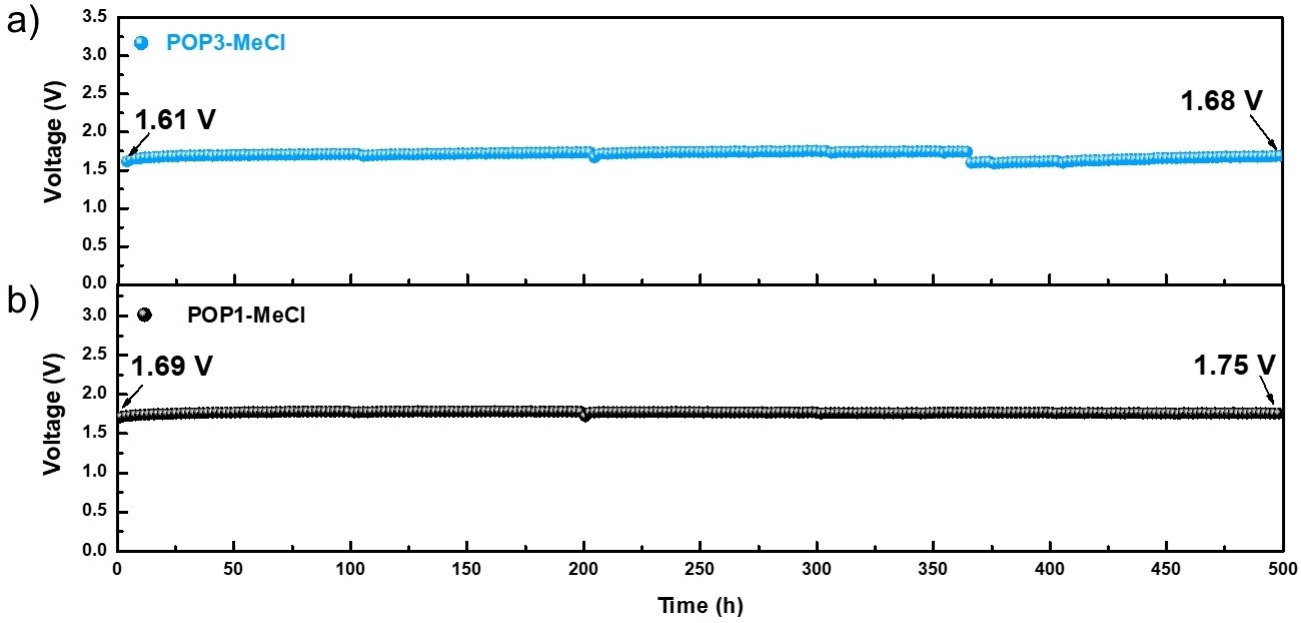

Figure 8. The in−situ durability of (a) POP3-based AEMWE and (b) POP1-based AEMWE operated at a constant current density of 0.7 A cm^{-2} under 60 °C for 500 h. PDTP AEM (25 μm), 2 mg cm^{-2} IrO_2 at the anode, 0.5 mg cm^{-2} PtRu/C at the cathode, 60 °C, 1 M KOH.

Supporting Information Summary

Additional characterization data.

Acknowledgments

This work was supported by Spain's Agencia Estatal de Investigación [Projects PID2019-109403RB-C22 (I/FEDER, UE), PID2019-109403RB-C21 and PID2020-118547GB-I00 (AEI/FEDER, UE)], by the Spanish Junta de Castilla y León (VA224P2). This work was also supported by the Nano·Materials Technology Development program (RS-2023-00235295) through the (NRF) funded by the Ministry of Science and ICT of South Korea. S.R.-M. thanks Spain's Ministry of Science, Innovation, and Universities for an FPU grant and a complementary FPU mobility aid.

Conflict of Interests

The authors declare no conflict of interest.

Data Availability Statement

The data that support the findings of this study are available from the corresponding author upon reasonable request.

Keywords: Alkaline membrane water electrolyzer · Ionomer · Porous organic polymers · High performance · Water splitting

[1] N. Du, C. Roy, R. Peach, M. Turnbull, S. Thiele, C. Bock, *Chem. Rev.* **2022**, *122*, 11830–11895.
[2] M. Chatenet, B. G. Pollet, D. R. Dekel, F. Dionigi, J. Deseure, P. Millet, R. D. Braatz, M. Z. Bazant, M. Eikerling, I. Staffell, P. Balcombe, Y. Shao-Horn, H. Schäfer, *Chem. Soc. Rev.* **2022**, *51*, 4583–4762.
[3] J. Bollmann, S. Pitchaimuthu, M. F. Kühnel, *Energies* **2023**, *16*, 3604.
[4] M. Nasser, T. F. Megahed, S. Ookawara, H. Hassan, *Environ. Sci. Pollut. Res. Int.* **2022**, *29*, 86994–87018.
[5] C. H. Park, S. Y. Lee, D. S. Hwang, D. W. Shin, D. H. Cho, K. H. Lee, T.-W. Kim, T.-W. Kim, M. Lee, D.-S. Kim, C. M. Doherty, A. W. Thornton, A. J. Hill, M. D. Guiver, Y. M. Lee, *Nature* **2016**, *532*, 480–483.
[6] C. Hu, N. Y. Kang, H. W. Kang, J. Y. Lee, X. Zhang, Y. J. Lee, S. W. Jung, J. H. Park, M. Kim, S. J. Yoo, S. Y. Lee, C. H. Park, Y. M. Lee, *Angew. Chem.* **2024**, *36*(3), e20231669710.1002/ange.202316697.
[7] C. Hu, J. Y. Lee, Y. J. Lee, S. H. Kim, H. Hwang, K. Yoon, C. Park, S. Y. Lee, Y. M. Lee, *Next Energy* **2023**, *1*, 100044.
[8] D. Li, E. J. Park, W. Zhu, Q. Shi, Y. Zhou, H. Tian, Y. Lin, A. Serov, B. Zulevi, E. D. Baca, C. Fujimoto, H. T. Chung, Y. S. Kim, *Nat. Energy* **2020**, *5*, 378–385.
[9] L. Wan, Z. Xu, P. Wang, P. F. Liu, Q. Xu, B. Wang, *Chem. Eng. J.* **2022**, *431*, 133942.
[10] S. Shiva Kumar, V. Himabindu, *Mater. Sci. Energy Technol.* **2019**, *2*, 442–454.
[11] A. Y. Faid, L. Xie, A. O. Barnett, F. Seland, D. Kirk, S. Sunde, *Int. J. Hydrogen Energy* **2020**, *45*, 28272–28284.
[12] N. Chen, C. Hu, H. H. Wang, S. P. Kim, H. M. Kim, W. H. Lee, J. Y. Bae, J. H. Park, Y. M. Lee, *Angew. Chem. Int. Ed.* **2021**, *60*, 7710–7718.
[13] J. Wang, Y. Zhao, B. P. Setzler, S. Rojas-Carbonell, C. Ben Yehuda, A. Amel, M. Page, L. Wang, K. Hu, L. Shi, S. Gottesfeld, B. Xu, Y. Yan, *Nat. Energy* **2019**, *4*, 392–398.
[14] N. Chen, H. H. Wang, S. P. Kim, H. M. Kim, W. H. Lee, C. Hu, J. Y. Bae, E. S. Sim, Y. C. Chung, J. H. Jang, S. J. Yoo, Y. Zhuang, Y. M. Lee, *Nat. Commun.* **2021**, *1*, 236710.1038/s41467-021-22612-3.
[15] N. Ul Hassan, M. Mandal, G. Huang, H. A. Firouzjaie, P. A. Kohl, W. E. Mustain, *Adv. Energy Mater.* **2020**, *10*, 1–8.
[16] P. Mardle, B. Chen, S. Holdcroft, *ACS Energy Lett.* **2023**, *8*, 3330–3342.
[17] D. S. Kim, A. Labouriau, M. D. Guiver, Y. S. Kim, *Chem. Mater.* **2011**, *23*, 3795–3797.
[18] J. Lim, J. M. Klein, S. G. Lee, E. J. Park, S. Y. Kang, S. Maurya, W. E. Mustain, S. Boettcher, Y. S. Kim, *ACS Energy Lett.* **2024**, *9*, 3074–3083.
[19] *Electrodes for Fuel Cells and Electrolyzers*, **2023**, US20230343969A1.
[20] S. D. Poynton, R. C. T. Slade, T. J. Omasta, W. E. Mustain, R. Escudero-Cid, P. Ocón, J. R. Varcoe, *J. Mater. Chem. A* **2014**, *2*, 5124–5130.

[21] C. Hu, Y. J. Lee, J. Y. Sohn, H. Hwang, S. W. Jung, Y. M. Lee, *J. Power Sources* **2024**, *599*, 234228.
[22] G. Huang, M. Mandal, N. U. Hassan, K. Groenhout, A. Dobbs, W. E. Mustain, P. A. Kohl, *J. Electrochem. Soc.* **2020**, *167*, 164514.
[23] S. Maurya, C. H. Fujimoto, M. R. Hibbs, C. Narvaez Villarrubia, Y. S. Kim, *Chem. Mater.* **2018**, *30*, 2188–2192.
[24] C. Hu, H. W. Kang, S. W. Jung, M. Liu, Y. J. Lee, J. H. Park, N. Y. Kang, M. Kim, S. J. Yoo, C. H. Park, Y. M. Lee, *Adv. Sci.* **2024**, *11*, 1–13.
[25] C. Hu, H. H. Wang, J. H. Park, H. M. Kim, N. Chen, Y. M. Lee, *J. Electrochem. Soc.* **2022**, *169*, 014515.
[26] B. Lopez-Iglesias, F. Suárez-García, C. Aguilar-Lugo, A. González Ortega, C. Bartolomé, J. M. Martínez-Ilarduya, J. G. de la Campa, Á. E. Lozano, C. Álvarez, *ACS Appl. Mater. Interfaces* **2018**, *10*, 26195–26205.
[27] B. S. Ghanem, M. Hashem, K. D. M. Harris, K. J. Msayib, M. Xu, P. M. Budd, N. Chaukura, D. Book, S. Tedds, A. Walton, N. B. McKeown, *Macromolecules* **2010**, *43*, 5287–5294.
[28] S. Rico-Martínez, C. Álvarez, A. Hernández, J. A. Miguel, Á. E. Lozano, *Membranes (Basel)* **2022**, *12*, 547.
[29] S. Rico-Martínez, A. Ruiz, B. López-Iglesias, C. Álvarez, Á. E. Lozano, J. A. Miguel, *ACS Appl. Polym. Mater.* **2024**, *6*, 2453–2463.
[30] C. Hu, J. H. Park, H. M. Kim, H. H. Wang, J. Y. Bae, N. Y. Kang, N. Chen, Y. M. Lee, *J. Membr. Sci.* **2022**, *647*, 120341.
[31] Y. Jia, L. Ma, Q. Yu, N. A. Qaisrani, L. Li, R. Zhou, G. He, F. Zhang, *Ionics* **2020**, *26*, 5617–5627.
[32] Y. Fan, J. Zhou, J. Chen, C. Shen, S. Gao, *Int. J. Hydrogen Energy* **2023**, *48*, 17630–17640.
[33] K. Tanaka, H. Kita, K. Okamoto, *Polymer (Guildf)* **1992**, *33*, 585–592.
[34] D. P. Leonard, M. Lehmann, J. M. Klein, I. Matanovic, C. Fujimoto, T. Saito, Y. S. Kim, *Adv. Energy Mater.* **2023**, *13*, 2203488, DOI 10.1002/aenm.202203488.
[35] E. J. Park, P. Jannasch, K. Miyatake, C. Bae, K. Noonan, C. Fujimoto, S. Holdcroft, J. R. Varcoe, D. Henkensmeier, M. D. Guiver, Y. S. Kim, *Chem. Soc. Rev.* **2024**, *53*, 5704–5780.
[36] E. J. Park, Y. S. Kim, *J. Mater. Chem. A* **2018**, *6*, 15456–15477.

Manuscript received: July 27, 2024
Revised manuscript received: September 4, 2024
Accepted manuscript online: September 5, 2024
Version of record online: ■■, ■■